(4+2) and (2+2) Cycloadditions of Benzyne to C_{60} and Zig-Zag Single-Walled Carbon Nanotubes: The Effect of the Curvature

Juan Pablo Martínez[a], Fernando Langa[b], F. Matthias Bickelhaupt[c,d], Sílvia Osuna[a,*] and Miquel Solà[a,*]

[a]Institut de Química Computacional i Catàlisi and Departament de Química, Universitat de Girona, Campus de Montilivi, 17071 Girona, Catalonia, Spain. E-mail: silvia.osuna@udg.edu; miquel.sola@udg.edu.
[b] Universidad de Castilla-La Mancha, Instituto de Nanociencia, Nanotecnología y Materiales Moleculares (INAMOL), Campus de la Fábrica de Armas, 45071 Toledo, Spain
[c] Department of Theoretical Chemistry and Amsterdam Center for Multiscale Modeling (ACMM), Vrije Universiteit Amsterdam, De Boeleaan 1083, NL-1081HV Amsterdam, The Netherlands.
[c] Institute of Molecules and Materials (IMM), Radboud University Nijmegen, The Netherlands.

Abstract

Addition of benzyne to carbon nanostructures can proceed via (4+2) (1,4-addition) or (2+2) (1,2-addition) cycloadditions depending on the species under consideration. In this work, we analyze by means of density functional theory calculations the reaction mechanisms for the (4+2) and (2+2) cycloadditions of benzyne to nanostructures of different curvature, namely, C_{60} and a series of zig-zag single-walled carbon nanotubes. Our DFT calculations reveal that, except for the concerted (4+2) cycloaddition of benzyne to zig-zag single-walled carbon nanotubes, all cycloadditions studied are stepwise processes with the initial formation of a biradical singly-bonded intermediate. From this intermediate, the rotation of the benzyne moiety determines the course of the reaction. The Gibbs energy profiles lead to the following conclusions: (i) except for the 1,4-addition of benzyne to a six-membered ring of C_{60}, all 1,2- and 1,4-additions studied are exothermic processes; (ii) for C_{60}, the (2+2) benzyne cycloaddition is the most favoured reaction pathway; (iii) for zig-zag single-walled carbon nanotubes, the (4+2) benzyne cycloaddition is preferred over the (2+2) reaction pathway; and (iv) there is a gradual decrease in the exothermicity of the reaction and an increase of energy barriers as the diameter of the nanostructure of carbon is increased. By making use of the activation strain model, it is found that the deformation of the initial reactants in the rate-determining transition state is the key factor determining the chemoselectivity of the cycloadditions with benzyne.

1 Introduction

Nanostructured allotropes of carbon such as fullerene C_{60} and carbon nanotubes (CNTs) encompass an active area of research in many fields of nanoscience and nanotechnology.[1–4] Three decades after its discovery,[5] fullerene C_{60} is still an attractive material due to its unique structure and specific properties.[6,7] Numerous derivatives can be synthesized from C_{60} with the purpose of promoting applications in biology,[8] medicine,[9] photovoltaics,[10] among others.[11,12] There is also a great interest in CNTs due to their large values of modulus of elasticity,[13,14] their high stability (they are stable up to 2800 ºC in vacuum and 750 ºC in air[15]), their thermal conductivity that is even better than that of some good thermal conductors like copper,[15,16] and their particular electronic and optical properties that, depending on their sidewall curvature, chirality, and local environment, can be similar to those of certain metals or semiconductors.[17–19] In view of that, it is not difficult to imagine the synthesis of interesting materials developed from CNTs taking advantage of their outstanding thermal and electrical properties combined with high specific stiffness and strength.[20,21] In fact, functionalized CNTs have been shown to be useful assemblies in fields of materials, medical and biological sciences.[22–24] However, the actual application of these nanomaterials is hampered because their selective purification is hard to achieve due to poor solubility of CNTs in conventional solvents or the formation of agglomerates because of their strong π-stacking tendencies.[25–27] These problems can be partially or totally solved with proper chemical modifications.[28–30] The most common chemical reactions used to functionalize carbon nanostructures are the Diels-Alder reaction, the 1,3-dipolar (Prato) cycloaddition, photochemical silylation, carbene and nitrene additions, Bingel-Hirsch reaction, and (2+2) cycloadditions.[31–36]

There is experimental evidence describing the chemical functionalization of fullerenes through (2+2) aryne cycloadditions (1,2-additions). To our knowledge, the first study of the reaction of fullerenes and benzyne was reported by Cooks *et al.*[37] already in 1992. These authors found that the (2+2) benzyne cycloaddition (BC) to C_{60} occurs at the [6,6] bonds of C_{60} (although they did not exclude the possibility of a [5,6] addition) to form mono-, di-, tri-, and tetra-adducts. Three years later, the group of Nogami[38] characterized by X-ray the adduct of the (2+2) cycloaddition of 4,5-dimethoxybenzyne to C_{60}. This adduct was shown to exhibit a benzocyclobutene structure attached to a closed [6,6] bond of C_{60}. In 2001, Nishimura *et al.* were able to synthesize, isolate and characterize eight regioisomers corresponding to all possible [6,6] bisadducts generated by the (2+2) bisaddition of 4,5-dimethoxybenzyne to C_{60}.[39] More recently, Yang *et al.*[40] claimed on the basis of NMR, UV-vis spectroscopy, and cyclic voltammetry, the formation of an unprecedented [5,6]-open adduct from the (2+2) cycloaddition of benzyne to C_{60}. In the case of C_{70}, the first studies were reported by the group of Taylor.[41,42] They found that C_{70} can accommodate up to 10 benzyne addends. From the ^{1}H NMR spectra they concluded that benzyne addition to C_{70} gives four possible monoadducts; three of them corresponding to (2+2) additions

to [6,6] bonds and one being the result of a (4+2) cycloaddition (1,4-addition) in a six-membered ring (6-MR). In 1998, Meier *et al.*[43] found by X-ray crystallography that one of the four monoadducts generated by the BC to C_{70} is a closed-cage [6,6] adduct. Two of the remaining three monoadducts were assigned to [6,6] bonds additions and the last one on the basis of ^{13}C NMR results was considered the result of a [5,6] attack to C_{70}. The first successful BC to endohedral metallofullerenes (EMFs) was carried out in Gd@C_{82} by Gu *et al.*[44] who reported the formation of two different (2+2) monoadducts. The addition of benzyne to La@C_{82} was shown to take place preferentially at the [5,6] bonds to yield close cyclobutene rings.[45] Echegoyen *et al.*[46] reported that the BC with $Sc_3N@I_h$-C_{80} produced two thermally stable cycloadducts corresponding to the addition of benzyne to both a [5,6] and a [6,6] bond as confirmed by the X-ray crystal structures. These bonds were found to be elongated but not broken in the resulting cycloadduct (i.e. the carbon-carbon distance is ~1.65 Å in the final product).[47] The (2+2) cycloaddition of $Sc_3N@I_h$-C_{80} with 4,5-diisopropoxybenzyne also yields two adducts that were assigned to the [6,6]- and [5,6]-regioisomers.[48] As far as we know, there is not a single experimental work reporting the (4+2) BC to (metallo)fullerenes. It has been claimed that small diameter carbon nanostructures like fullerenes promote better the (2+2) cycloaddition.[37,39]

Within the chemical functionalization of CNTs, some proposals to reach covalent junctions between functional groups and nanotubes have been already provided.[49–52] In the case of the BC to CNTs, more than one decade ago it was suggested that the addition of arynes to single-walled CNTs (SWCNTs) could lead to the synthesis of paddle-wheel-like nanostructures.[53] Later Langa and coworkers[27,54] published the reaction between benzyne and SWCNTs under microwave irradiation with a high degree of functionalization. The authors found that aryne addition increases the mass of SWCNTs by a factor ranging from 5% to 19%, confirming thus the functionalization of these materials. In view of that, Nagase and coworkers[55] recently described energy profiles of the (4+2) and (2+2) BC to armchair SWCNTs based on density functional theory (DFT) methodology. They determined that the (4+2) cycloaddition of benzyne in a slanted position is the most favorable for large diameters of the nanotube. For small diameters (<10 Å), the (2+2) addition in a slanted bond is preferred thermodynamically; yet kinetically the most favorable attack is the one in the perpendicular position.

In summary, benzyne reacts with fullerenes and EMFs through (2+2) cycloadditions that occur preferentially at [6,6] bonds, although there are several examples of [5,6] attacks. For SWCNTs, cycloadditions of benzyne can produce both (2+2) and (4+2) adducts depending on the shape and curvature of the nanotube, as well as their intrinsic electronic nature. The mechanistic details of the BC to all these nanostructures of carbon have not been entirely elucidated yet and the reasons for the chemoselectivity (preference of the (2+2) over the (4+2) BC) and regioselectivity (the [6,6] attack is more frequently found than the [5,6] addition in fullerenes) of the BCs have not

been discussed to date. In this contribution, we aim to provide a comprehensive description and analysis of the chemo- and regioselectivity of the BC to different nanostructures of carbon. First, we present a study of both (4+2) and (2+2) additions to fullerene C_{60}. A generalization of the reaction mechanisms occurring in C_{60} is summarized in Scheme I; wherein we have included terminology that is useful to identify every structure discussed through the whole manuscript. After defining the potential energy surface for the benzyne cycloaddition (PES-BC) to C_{60}, we discuss the PES-BC of the (4+2) and (2+2) BC to zig-zag SWCNTs. An equivalent terminology as defined in Scheme I is also used in the description of the reaction mechanisms studied for zig-zag SWCNTs. We do not consider armchair SWCNTs because their reaction pathways were already discussed in the work by Nagase and coworkers.[55] The effect of the sidewall curvature on the chemical reactivity of the nanostructures has been directly analyzed. To that aim, we have investigated both (4+2) and (2+2) additions to carbon nanostructures whose diameter ranges from 14.1 Å (large-diameter zig-zag SWCNT) to 6.8 Å (i.e. fullerene C_{60}).

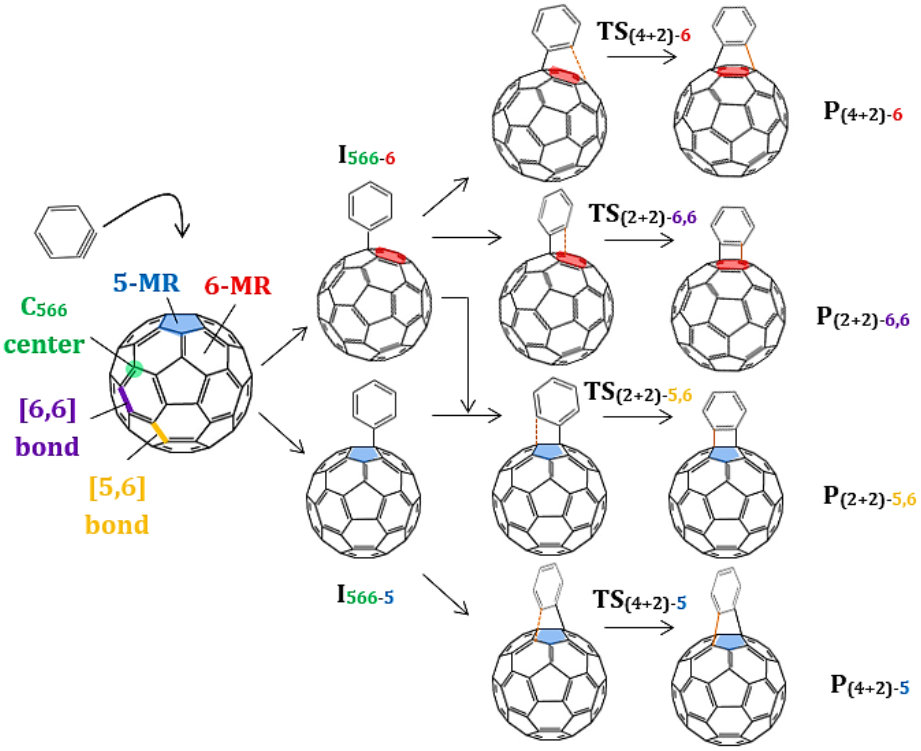

Scheme 1. Generalized representation of the reaction mechanisms studied in the current manuscript. Biradical singly-bonded intermediates are represented as **I**; transition states and final products are labeled as **TS** and **P**, respectively. Two subscripts separated by a dash are used to indicate how the species are formed; in fact, they refer to chemoselectivity-regioselectivity. The left subscript takes the values of "(4+2)" and "(2+2)" to denote whether the 1,4- or 1,2-addition takes place, respectively; but it also acquires the value of "566" indicating the formation of biradical singly-bonded structures related to the attack on a 566 carbon center (i.e. a C_{566} center, see green dot in the fullerene structure). The right subscript takes the values of "5" and "6" to indicate whether a 5 or 6-membered ring (see 5-MR in blue, and 6-MR in red) is under attack; but it can also have the values of "5,6" and "6,6" to denote whether a [5,6] or [6,6] bond is attacked (see respectively orange and purple labels). An analogous terminology is used for SWCNTs.

2 Methodology

All DFT calculations were performed using the Amsterdam Density Functional (ADF) program.[56] Molecular orbitals (MOs) were expanded in terms of an uncontracted set of Slater-type orbitals (STOs) of double-ζ (DZP) and triple-ζ (TZP) quality containing diffuse functions and one set of polarization functions. STOs correctly describe the asymptotic, long-range and near-the-nucleus (cusp) behaviors. However, their evaluation for systems with many tens of atoms can be computationally very expensive; therefore the frozen-core approximation[56] was used, which freezes the core orbitals (i.e. the orbital *1s* of the carbon atoms) during the self-consistent field procedure. It was shown that the frozen core approximation has a negligible effect on the optimized equilibrium geometries.[57,58] Scalar relativistic corrections were also included self-consistently by using the zeroth order regular approximation (ZORA).[59,60]

Energies and gradients were calculated via the local density approximation (Slater exchange) with non-local corrections for exchange (Becke88)[61] and correlation (Perdew86)[62] (i.e. the BP86 functional). Moreover, energy dispersion corrections as developed by Grimme[63] (D_2) were added to the DFT energy. It has been shown that dispersion corrections are essential for a correct description of the thermodynamics and kinetics of reactions with fullerenes and nanotubes.[64] For open-shell systems, unrestricted calculations with broken symmetry were performed. This is particularly important in the case of biradical intermediates.

Geometry optimizations without symmetry constraints and analytical frequency calculations were performed in the gas phase at the BP86-D_2/DZP level of theory. Electronic energies were obtained in the gas phase with the TZP basis at the geometries optimized with the DZP basis (i.e. BP86-D_2/TZP//BP86-D_2/DZP). In the search of stationary points, the QUILD code (quantum regions interconnected by local descriptions)[65] was used. QUILD works as a wrapper around the ADF program; it creates input files for ADF, then executes the program and collects energies and gradients generated by ADF. In addition, the efficiency of QUILD is reflected in the use of techniques such as adapted delocalized coordinates and the fact that this code constructs model Hessians with the appropriate number of eigenvalues.[66] This latter feature is particularly useful for the search of transition state (TS) structures.

Relative Gibbs energies (ΔG) were determined from electronic energies at the BP86-D_2/TZP//BP86-D_2/DZP level of theory together with corrections of zero-point energies, thermal contributions to the internal energy, and entropy determined in the gas phase at 298 K with the BP86-D_2/DZP method considering an ideal gas in standard conditions. It is likely that the entropy term may be overestimated by our gas-phase calculations based on harmonic frequencies; although we expect a comparable error for the different reaction pathways and, therefore, comparisons should not be affected by this possible overestimation of the entropy correction.[67]

Solvent effects were not included in the present calculations since the BC is usually carried out in rather nonpolar solvents. The absence of charge-separated species along the reaction coordinate suggests that solvent effects are unimportant in this reaction.

Finally, in the Supporting Information we provide a detailed description of the construction of the SWCNT models to be used in computational modeling (see Figure S1 and additional explanation; as well as see Table S1 and Figure S2 and discussion for a comparative study of the benzyne cycloaddition to SWCNT constructed with different approaches). Moreover, for all structures we make sure that the number of cells is suitable for the purpose of our study; i.e. electronic properties such as electronic energies were conveniently converged with respect to the size of the implemented model (see Table S2 and associated discussion).

3 Results and Discussion

This section is divided into two parts. Part I contains a detailed study of the BC to C_{60} with an exhaustive description of the different reaction pathways. Then, by making use of the information of Part I, in Part II the reaction mechanisms for zig-zag SWCNTs are reported. The introduction of nanotubes of different diameter enables us to discuss the curvature effect of sidewall BC to different nanostructures of carbon. The effect of the curvature is studied with activation strain analyses at the transition state of the (2+2) and (4+2) reactions.

I. Benzyne cycloaddition to C_{60}

As far as we know, a detailed mechanistic study of the BC to C_{60} has not been consistently established yet. We, therefore, explore the PES-BC to C_{60} considering the four possible cycloadducts produced from the 1,2-addition to [5,6] and [6,6] bonds and the 1,4-addition to 5- and 6-MRs. The Gibbs energy profile in terms of changes in Gibbs energies for the formation of the four different adducts is depicted in Figure 1.

In the first stage of the reaction mechanism, a reactant complex (**RC**) is formed in which the main interactions between benzyne and C_{60} are noncovalent.[68] We distinguish two arrangements of benzyne with respect to the fullerene surface, $\mathbf{RC_{ds}}$ and $\mathbf{RC_T}$; subscripts *ds* and *T* standing for displaced sandwiched and T-shaped configurations as schematized in Figure 1. Nevertheless, a detailed analysis of the structure and energy of those species is provided in figures S3 and S4 in the Supporting Information. In the first TS structure, namely $\mathbf{TS_{566\text{-}6}}$, benzyne is attacking a C atom in the ring junction between one five-member ring (5-MR) and two six-member rings (6-MRs) of C_{60} to generate a biradical singly-bonded intermediate $\mathbf{I_{566\text{-}6}}$. In both the TS and intermediate, the C≡C of benzyne is oriented toward a 6-MR of the cage as shown in Scheme 1.

$TS_{566\text{-}6}$ has a small imaginary frequency due to the flatness of the PES-BC, 23.2i cm^{-1}, with a normal mode that suggests a reaction progress toward an intermediate structure with biradical character in which only one carbon in benzyne is covalently attached to a C_{566} center. The ability of benzyne to rotate in a very flat surface also gives rise to the formation of an orientational isomer, **$I_{566\text{-}5}$** isoenergetic to **$I_{566\text{-}6}$**. More importantly, the description of the (2+2) and (4+2) BC to C_{60} can be consistently done from the idea of a rotating benzyne; being the formation of biradical singly-bonded intermediate structures the rate-determining step of the (2+2) reaction (but not for the (4+2) addition, see Figure 1). For all singly-bonded intermediates and transition states, we determine that triplet ($<S^2>\approx2.0$) and open-shell singlet ($<S^2>\approx1.0$) biradical structures present similar energies (absolute energy differences of *ca*. 0.5 kcal/mol) indicating a weak spin coupling between the unpaired electrons of the two fragments. However, these energy comparisons are done at the open-shell singlet optimized geometry, therefore we deduce that a geometry relaxation for the triplet state could slightly stabilize it and, consequently, the ground state for biradical singly-bonded structures could be the triplet state. Additionally, it is worth mentioning that small deformations of spherical C_{60} can bring about an appearance of fine structure in the electronic energy spectrum as compared to the spherical case.[69] Still, we assume that the system follows the singlet potential energy surface through the entire reaction pathway since the singlet-to-triplet spin-crossing is expected to be not allowed due to the small spin-coupling term of the dipole moment of the transition integral. In fact, the major change between the open-shell singlet and triplet spin densities is located in the two radical carbon atoms. Additional information in the electronic structure and spin-orbit interactions for carbon nanostructures can be found in the works by Ando[70] and Pincak *et al*.[71–73]

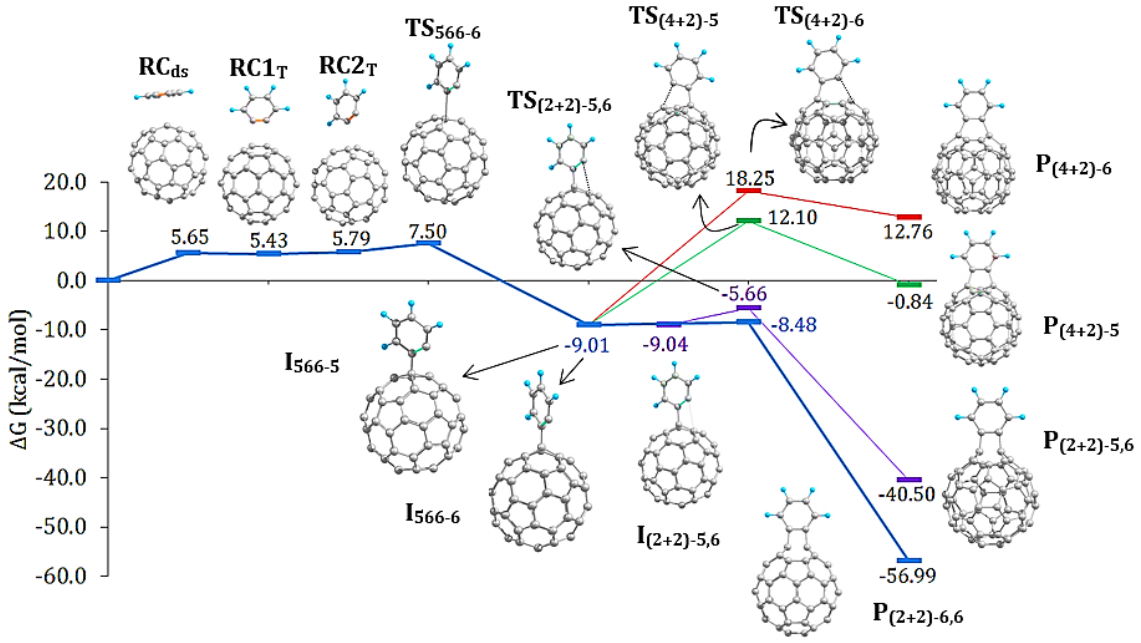

Figure 1. Gibbs energy profile (in kcal/mol) for the (2+2) (in blue and purple) and (4+2) (in red and green) benzyne cycloadditions to fullerene C_{60}. The energy for the transition state for the rotation toward a [6,6] bond marked with a star (*), **TS**$_{(2+2)-6,6}$, corresponds to a linear-transit maximum point (see Figure 2). Blue and purple colored ΔG values stand for open-shell singlet structures.

As mentioned earlier, the biradical singly-bonded intermediate **I**$_{566-5}$ and **I**$_{566-6}$ structures are the key structures leading to the different cycloadducts: **I**$_{566-5}$ presents the benzyne faced to a 5-MR, and thus it is the precursor of the 1,4-addition to a pentagonal ring; whereas **I**$_{566-6}$ faced to 6-MR leads to the formation of 6-MR-based cycloadducts. At these points, the (4+2) addition of benzyne can take place via **TS**$_{(4+2)-5}$ or **TS**$_{(4+2)-6}$ to yield **P**$_{(4+2)-5}$ and **P**$_{(4+2)-6}$, respectively. The (4+2) BC to C_{60} is kinetically hampered in view of the larger energy barriers (more than 20 kcal/mol) as compared to its (2+2) BC counterpart. Moreover, the formation of **P**$_{(4+2)-6}$ is an endergonic process.

The possible rotation of benzyne in the intermediate structures is now evaluated to formulate a mechanistic pathway leading to the (2+2) cycloadducts as schematized in Figure 2a. Coincidently the rotating-benzyne mechanism has been formulated very recently for EMFs by Zhao et al.[74] There are two types of bonds to be attacked: [5,6] and [6,6] bonds. From **I**$_{566-5}$, only [5,6] bonds can be attacked to achieve the product resulting from the (2+2) BC, **P**$_{(2+2)-5,6}$. Nevertheless, from **I**$_{566-6}$ both types of bonds are available to react giving rise to either **P**$_{(2+2)-5,6}$ or **P**$_{(2+2)-6,6}$. This situation shows that [5,6] adducts in C_{60} are statistically favored. We have performed linear transit (LT) calculations to assess the energetic cost for the rotation of benzyne in the biradical singly-bonded intermediates (see Figure 2b, 2c, and 2d). Our LT results indicate that the carbon-carbon bond between benzyne and C_{60} in both structures **I**$_{566-6}$ and **I**$_{566-5}$ can freely rotate since the rotation

occurs in a practically barrierless process. In Figure 2 the dihedral angle φ is monitored in order to describe the benzyne rotation. Bonds [6,6] and [5,6] are defined at φ=0º and φ=124º, respectively. In this context, φ in $\mathbf{I_{566\text{-}6}}$ must be decreased from 103º to 0º so as to reach a [6,6] bond. The maximum point of the linear transit toward a [6,6] bond is given at φ=50º and it provides an upper bound limit representing an energy barrier of 0.53 kcal/mol (see Figure 2b). This energetic cost is reported in Figure 1 as $\mathbf{TS_{(2+2)\text{-}6,6}}$. This small energy barrier for the (2+2) addition towards the [6,6] bond demonstrates that the rate-determining step for this process is given by the precursor $\mathbf{TS_{566\text{-}6}}$. For the (2+2) BC to a [5,6] bond we were able to locate another biradical singly-bonded intermediate, $\mathbf{I_{(2+2)\text{-}5,6}}$, resulting from the rotation of benzyne toward a [5,6] bond (φ=124º) from either $\mathbf{I_{566\text{-}6}}$ (φ=103º) or $\mathbf{I_{566\text{-}5}}$ (φ=174º) (see respectively figures 2c and 2d). This rotation does not lead to a ring closure as observed for [6,6]. Unlike the barrierless ring closure on a [6,6] bond, the course of the (2+2) BC is slightly hampered by an energy barrier of 3.4 kcal/mol characterized by a true transition state associated to the 4-membered ring closure, $\mathbf{TS_{(2+2)\text{-}5,6}}$.

Our complete analysis of the (4+2), and (2+2) cycloaddition to C_{60} indicate that the (2+2) BC to the [6,6] bond of C_{60} is the most kinetically and thermodynamically favored reaction pathway. However, the difference in Gibbs energy barriers between [5,6] and [6,6] additions is small; as a result we do not entirely discard the possibility of observing the (2+2) BC on a [5,6] bond. These results are in line with the experimental observation that only (2+2) BC are observed in fullerenes and that both [6,6] and [5,6] additions have been reported in the literature, with the [6,6] addition being more frequently observed than the [5,6] one.[37,38,40–42]

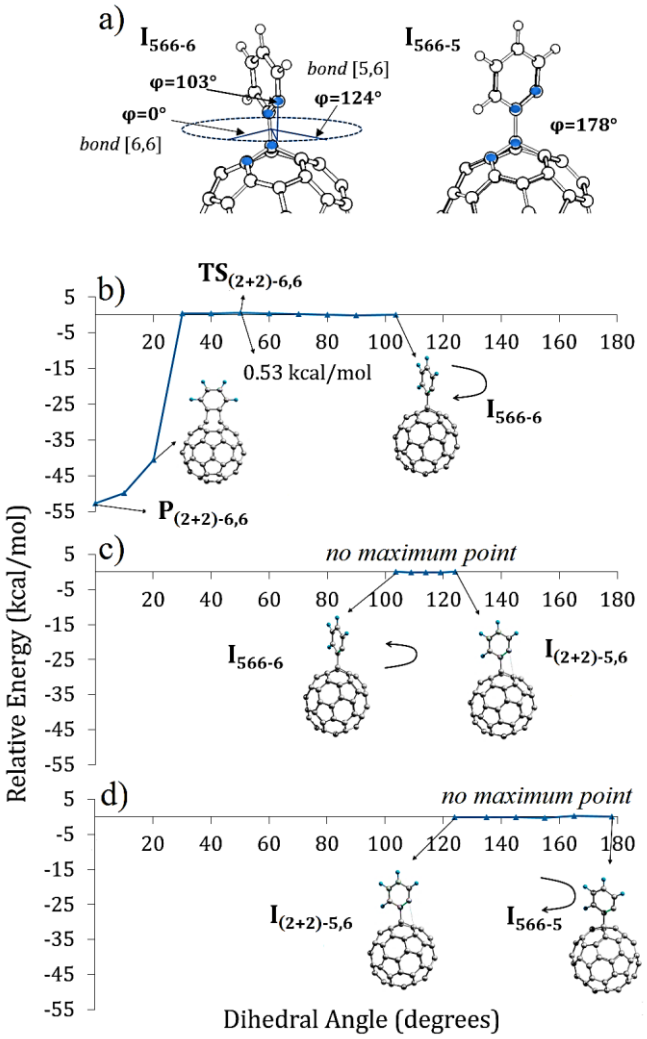

Figure 2. Schematic representation of the rotation of benzyne through stationary structures before ring closure. a) For **I** structures, a dihedral angle φ is defined by the two carbon atoms in a [6,6] bond and the two aryne ones (blue-marked). b) Linear transit (LT; relative energy with respect to $\mathbf{I}_{566}$) for the rotation of benzyne from $\mathbf{I}_{566\text{-}6}$ toward a [6,6] bond; c) LT for the rotation of benzyne from $\mathbf{I}_{566\text{-}6}$ toward a [5,6] bond; d) LT for the rotation of benzyne from $\mathbf{I}_{566\text{-}5}$ toward a [5,6] bond.

We have also investigated the possible open-cage structure of $\mathbf{P}_{(2+2)\text{-}5,6}$ and $\mathbf{P}_{(2+2)\text{-}6,6}$. Our results suggest that an open-cage structure of $\mathbf{P}_{(2+2)\text{-}6,6}$ is not possible since we were not able to locate any structure with a long (> 2 Å) attacked C–C [6,6]-bond. Nevertheless, an open-cage $\mathbf{P}_{(2+2)\text{-}5,6}$ was characterized to be a local-minimum structure; yet the Gibbs energy in this structure is 4.3 kcal/mol above the energy of its closed-cage counterpart. Besides, the maximum point of a linear transit going from closed to open cage is calculated at 5.6 kcal/mol (see Figure S5 in the Supporting Information). The structural deformation in the open-cage $\mathbf{P}_{(2+2)\text{-}5,6}$ is significantly larger than that of the closed-cage cycloadduct (by 57.3 kcal/mol). This is partially but not fully compensated by the large interaction energy in open-cage $\mathbf{P}_{(2+2)\text{-}5,6}$ due to better frontier orbital interactions among the deformed benzyne and C_{60} moieities.[75] We conclude that a closed-cage

product is more likely to be observed. In this regard, our results resemble the work of Iyoda *et al.*,[38] wherein the closed-cage product on a [6,6] bond is the most stabilized cycloadduct and it can be produced with a low-energy barrier; even though it is also suggested that the BC on a [5,6] may be kinetically competitive. On the other hand, when the reactant is 4,5-dibuthoxybenzyne, Yang *et al.*[40] suggested the formation of an open-cage [5,6] cycloadduct based on indirect evidence taken from ^{1}H and ^{13}C NMR, UV-vis spectra, and cyclic voltammetry results. From our calculations and taking into account similar experimental evidence,[38,47] we conclude that the BC to C_{60} can be conducted toward the formation of both cycloadducts $\mathbf{P}_{(2+2)\text{-}6,6}$ and $\mathbf{P}_{(2+2)\text{-}5,6}$ but we cannot support the hypothesis of open-cage structures.

II. Benzyne cycloaddition to SWCNTs and the curvature effect

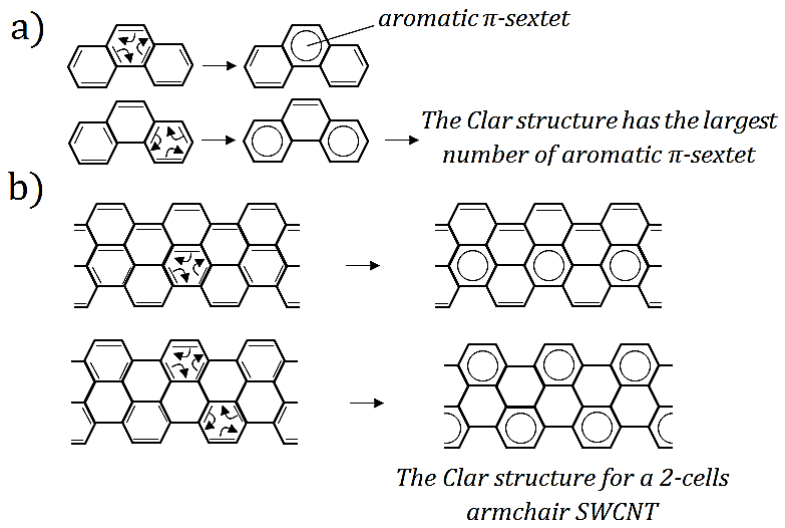

Scheme 2. Graphical representation of the Clar's aromatic π-sextet rule in a) phenantrene, and b) a 2-cell armchair SWCNT. The rule states that a Clar structure is the one with the largest number of aromatic π-sextets. For a given polycyclic aromatic hydrocarbon (PAH), the Clar structure is the structure that better agrees with the experimental behavior of the PAH.

Models designed to construct SWCNTs under the Clar theory have been named finite-length Clar cells (FLCC) and we refer the reader to the seminal papers dealing with this subject.[76–80] In this regard, we make use of complete Clar networks, which are fully benzenoid structures (see Scheme 2). These structures are more stable than their counterpart Kekulé structures as aromaticity provides stability to conjugated systems due to the nature of molecular orbitals.[51,81–84] However, by taken into consideration a molecular orbital model based on orbital-overlap arguments, the aromatic character of molecular systems involving π electrons has been purposed to be strongly influenced by the geometry of the ring structure; as a result a regular or distorted geometrical

arrangement indeed affects the aromaticity, or antiaromaticity, in the system.[85,86] In addition, complete Clar network models for SWCNTs are fully benzenoid structures, have closed-shell singlet ground states (at variance with many non-FLCC) and reach faster convergence in their electronic properties with respect to the number of cells of the nanotube than conventional models for SWCNTs. In this FLCC classification we select three different structures: (9,0)-, (12,0)- and (18,0)-SWCNT. Additionally, we include some FLCC structures lacking completeness of the Clar network such as (8,0)- and (13,0)-SWCNT. All models are represented in Figure 3.

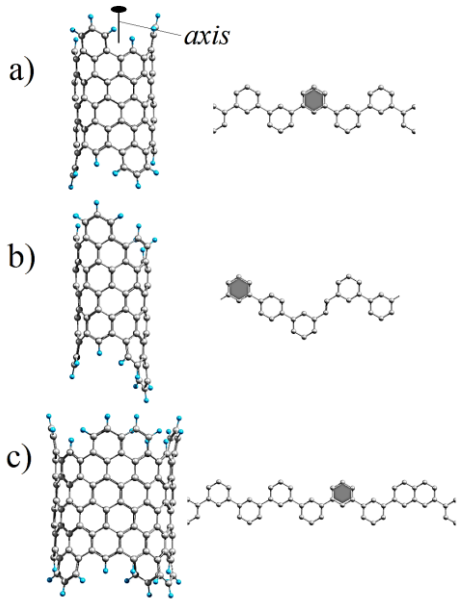

Figure 3. Finite-length Clar 3-cells models and unit cells for a) (9,0)-SWCNT; b) (8,0)-SWCNT; and c) (13,0)-SWCNT. Models for (12,0)- and (18,0)-SWCNT follow the same structural pattern as (9,0)-SWCNT. Benzenoid centres studied in this contribution are highlighted with a gray-filled hexagon. Dangling bonds are saturated with hydrogen atoms.

The BC to (9,0)-SWCNT is firstly described since the mechanistic details are exactly the same for all considered SWCNTs. As can be seen in Figure 4, the reaction starts with the formation of $\mathbf{RC_{ds}}$ (a true local-minimum point in the PES-BC) followed by TS structures for either the (4+2) or (2+2) BC. We were not able to optimize a $\mathbf{RC_T}$ structure. Like the BC to C_{60}, we confirmed $\mathbf{TS_{666\text{-}6}}$ to be a transition structure with a frequency of 254.3i cm^{-1} associated to a normal mode connecting $\mathbf{RC_{ds}}$ and the intermediate structure $\mathbf{I_{666\text{-}6}}$. To reach $\mathbf{TS_{666\text{-}6}}$, benzyne has to be approximated to the nanotube surface with one of the aryne carbon atoms at a distance of 2.01 Å and a dihedral angle (as described in Figure 5a) of φ=66º. The formation of the intermediate structure $\mathbf{I_{666\text{-}6}}$ has a Gibbs energy barrier of 9.8 kcal/mol. Observe that both $\mathbf{TS_{666\text{-}6}}$ and $\mathbf{I_{666\text{-}6}}$ present one of the aryne carbon atoms oriented toward a C_{666} centre of the nanotube, and the other one toward a 6-MR (following the definitions introduced in Scheme 1). Therefore, the benzyne rotation observed in the case of C_{60} to yield the different cycloadducts also occurs in SWCNTs.

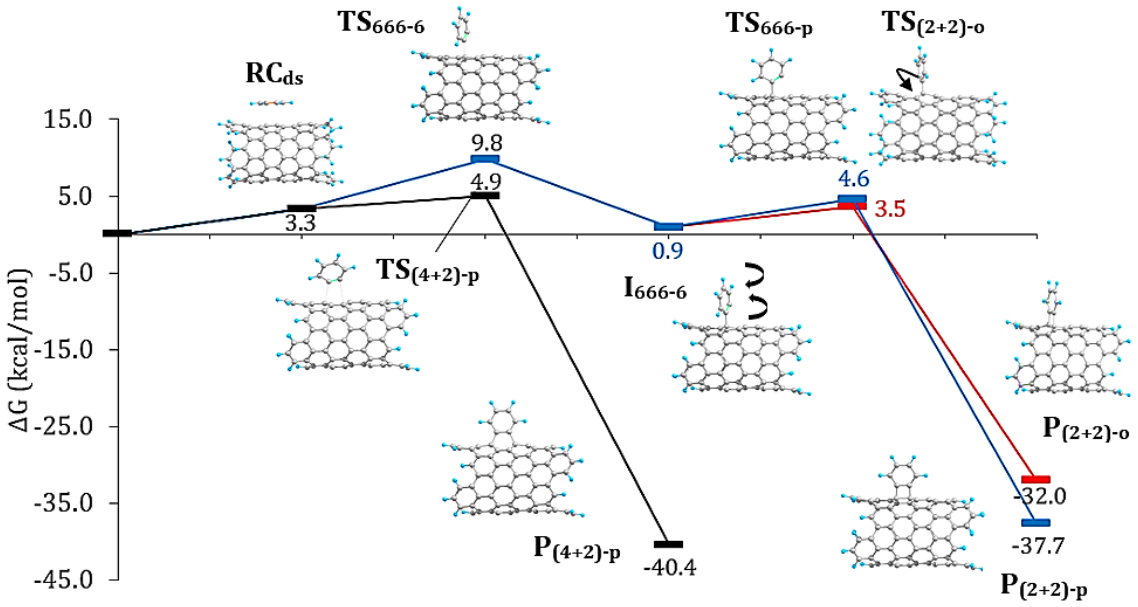

Figure 4. Gibbs energy profiles for the (2+2) (for blue and red lines benzyne is respectively added in parallel and oblique position with respect to the nanotube axis) and (4+2) (black line) benzyne cycloadditions to (9,0)-SWCNT. Blue and red coloured ΔG values stand for open-shell singlet structures.

Once the biradical singly-bonded intermediate **I$_{666\text{-}6}$** is formed, the final (2+2) cycloadduct formation can take place via two different pathways: the attack of benzyne following a parallel orientation "p" with respect to the nanotube axis (shown in blue in Figure 4), or in an oblique fashion "o" (in red, Figure 4). One could therefore postulate the formation of the two possible intermediates that arise from these two orientations, i.e. **I$_{(2+2)\text{-}p}$** or **I$_{(2+2)\text{-}o}$**. The former could not be, however, characterized since the (2+2) BC evolves toward the ring closure before the rotation of benzyne in **I$_{666\text{-}6}$** is completed (check LT calculations in Figure S6). As a matter of fact, the biradical singly-bonded intermediate **I$_{666\text{-}6}$** localizes benzyne with a distance of 1.54 Å and φ=100º and the rotation toward a parallel position means reducing φ to 0º. Analogously, the oblique position is found at φ=120º. In the case of a (2+2) BC in parallel orientation, we in fact optimized a first-order saddle point at φ=19º. The vibrational frequency calculation confirmed a small negative frequency of 75.3i cm^{-1} due to the flatness of the PES-BC; and the associated normal mode suggests that this is a transition state for the rotation of benzyne from **I$_{666\text{-}6}$** toward the parallel position (i.e. **TS$_{666\text{-}p}$**). Nonetheless, the small energy barrier of 3.7 kcal/mol calculated with **TS$_{666\text{-}p}$** indicates that the reaction evolves to the formation of **P$_{(2+2)\text{-}p}$** practically in a barrierless process (see details in Figure S6); thus **I$_{(2+2)\text{-}p}$** and **TS$_{(2+2)\text{-}p}$** could not be characterized. In the case of the oblique position, we optimized another first-order saddle point at φ=105º, but with the unbounded carbon atom in benzyne closer to the unbounded carbon atom in (9,0)-SCWNT (2.44 Å; this distance is 2.86 Å in **I$_{666\text{-}6}$**). The vibrational frequency calculation confirmed a negative frequency of 279.5i cm^{-1} associated to a normal mode resembling a ring

closure; therefore we distinguish this structure as a true transition state for the ring closure of the (2+2) BC in oblique position, $\mathbf{TS_{(2+2)\text{-}o}}$. Since $\mathbf{TS_{(2+2)\text{-}o}}$ is not exactly localized at the oblique position (φ=120º) we deduce that the reaction can proceed without previous formation of $\mathbf{I_{(2+2)\text{-}o}}$. The energy barrier calculated with $\mathbf{TS_{(2+2)\text{-}o}}$ is also small, 2.6 kcal/mol, thus concluding that the (2+2) BC can equally proceed at parallel and oblique positions.

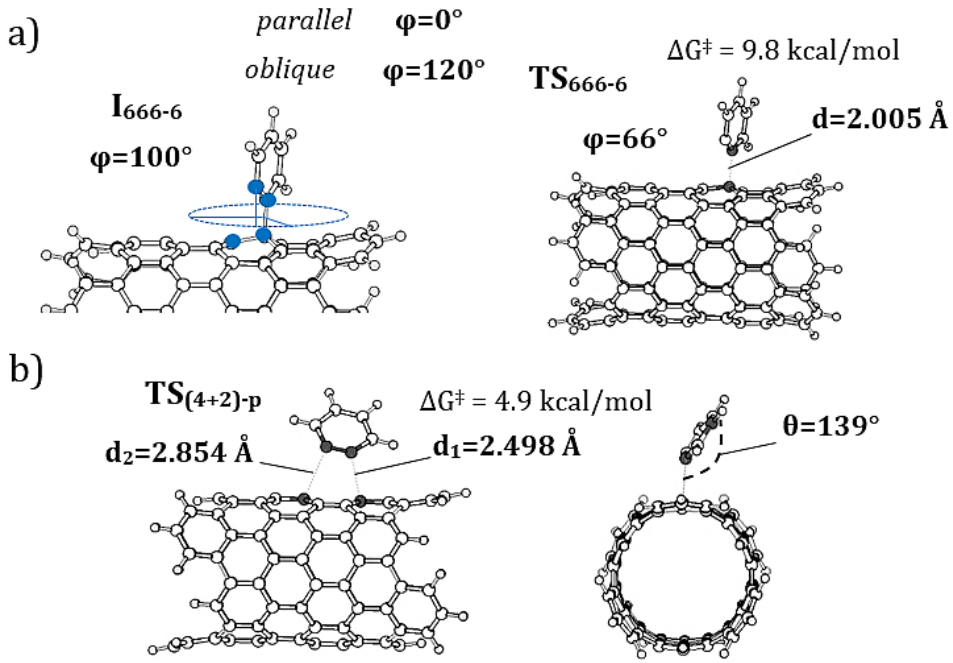

Figure 5. Schematic representation of the rotation and bent orientation of benzyne in the different stationary structures before ring closure occurs. a) A dihedral angle φ is defined by the four blue-marked carbon atoms and used in the structural description of intermediate and transition state structures through the (2+2) BC. b) A tilt angle θ is depicted and used in the structural description of the (4+2) BC. Gibbs energy barriers $\Delta G^{\ddagger}$ and some relevant distances are given between black-marked carbon atoms for TSs.

In the case of the (4+2) BC, $\mathbf{P_{(4+2)\text{-}o}}$ is highly destabilized since its energy lies 9.2 kcal/mol above the energy of the reactants; consequently benzyne can only add to the parallel position with respect to the nanotube axis. In this regard, a TS structure was also obtained (with an imaginary frequency of 39.6i cm^{-1}, see linear transit in Figure S7 in the Supporting Information). In $\mathbf{RC_{ds}}$, benzyne is completely tilted with θ=89.9º (the tilt angle θ is defined in Figure 5b) and the aryne carbon atoms are localized at 3.27 Å from the nanotube surface. To reach $\mathbf{TS_{(4+2)\text{-}p}}$ the tilt angle is reduced (θ=139.1º) and benzyne is approximated to the nanotube surface at a distance of 2.50 Å, which is longer than the distance in $\mathbf{TS_{666\text{-}6}}$ (compare figures 5a and 5b). The structure $\mathbf{TS_{(4+2)\text{-}p}}$ depicted in Figure 5b is a concerted transition state leading to $\mathbf{P_{(4+2)\text{-}p}}$ with a Gibbs energy barrier of only 4.9 kcal/mol. We conclude therefore that the (4+2) BC to (9,0)-SWCNT in parallel position is both kinetically and thermodynamically favored. This notwithstanding, the binding energies of benzyne to (9,0)-SWCNT for the (4+2) and (2+2) differ only by a few kcal/mol as reported recently by Vasiliev *et al*. in a series of zig-zag SWCNT.[87]

The mechanism as formulated in (9,0)-SWCNT can be also applied for the rest of the structures under consideration. In Table 1 we report reaction energies (ΔE) for the formation of benzyne cycloadducts as well as the initial activation energy E_a^1 (i.e. the energy barrier from the reactant complex to the following TS). Results in Table 1 demonstrate that the (4+2) BC is always the preferred reaction pathway for finite-diameter zig-zag SWCNTs because of the substantially lower E_a^1. It is also observed that the larger the curvature of the SWCNT, the lower the energy barriers and the larger the exothermicity[87] of the (2+2) and (4+2) additions. Moreover, $\mathbf{P_{(4+2)\text{-}p}}$ is the most stabilized product in all the cases, and thus the kinetics and thermodynamics correspond to the same addition.

We also investigated the mechanistic details of the BC to non-benzenoid centers like those reaction sites found at (8,0)- and (13,0)-SWCNTs and nonFLCC structures (the latter being zig-zag SWCNTs uniformly cut at the tube-ends with a high-spin ground state and electron localization at the edges). We reach the conclusion that the (4+2) BC in parallel position to non-benzenoid centers and nonFLCC models of (*n*,0)-SWCNTs is still favored (see figures S2 and S8 and tables S1 and S3 and discussion in the Supporting Information for complete details).

Table 1. Initial activation energies (E_a^1) and reaction energies (ΔE) in terms of electronic energy (kcal/mol) as a function of the diameter of the structure (Å).[a]

(*n*,*m*)	diameter	E_a^1		ΔE	
		(4+2)	(2+2)	(4+2)	(2+2)
(8,0)	6.26	1.25	4.74	-61.68	-59.49
(9,0)	7.05	1.32	5.67	-57.39	-53.92
(12,0)	9.39	2.36	7.94	-47.88	-45.17
(13,0)	10.18	2.42	7.81	-47.28	-42.61
(18,0)	14.09	5.22	8.90	-39.54	-37.81

[a] ΔE is the energy difference between products and reactants.
E_a^1 is the energy difference between the first transition state and the reactant complex.

Nagase and co-workers[55] concluded that the activation energy for large-diameter (*n*,*n*)-SWCNTs is lower for the (4+2) BC; but the (2+2) products are the most stable. Our results in Table 1 show that a gradual increase of the diameter of the SWCNT causes a steady increase in E_a^1 and ΔE for both types of BC. This trend resembles the tendency observed by Nagase *et al*.[55] In zig-zag SWCNTs, however, the (4+2) addition is for all diameters preferred kinetically and thermodynamically over the (2+2) one.

To explain changes in reactivity due to the curvature of the nanostructure, we make use of the activation strain model, ASM,[88–91] also known as distortion/interaction model.[92–94] ASM is a

helpful tool to better understand the origin of energy barriers. These barriers are analyzed in terms of strain and interaction energies between fragments participating in the formation or rupture of chemical bonds. Figure 6 schematizes the ASM for the BC to (9,0)-SWCNT.

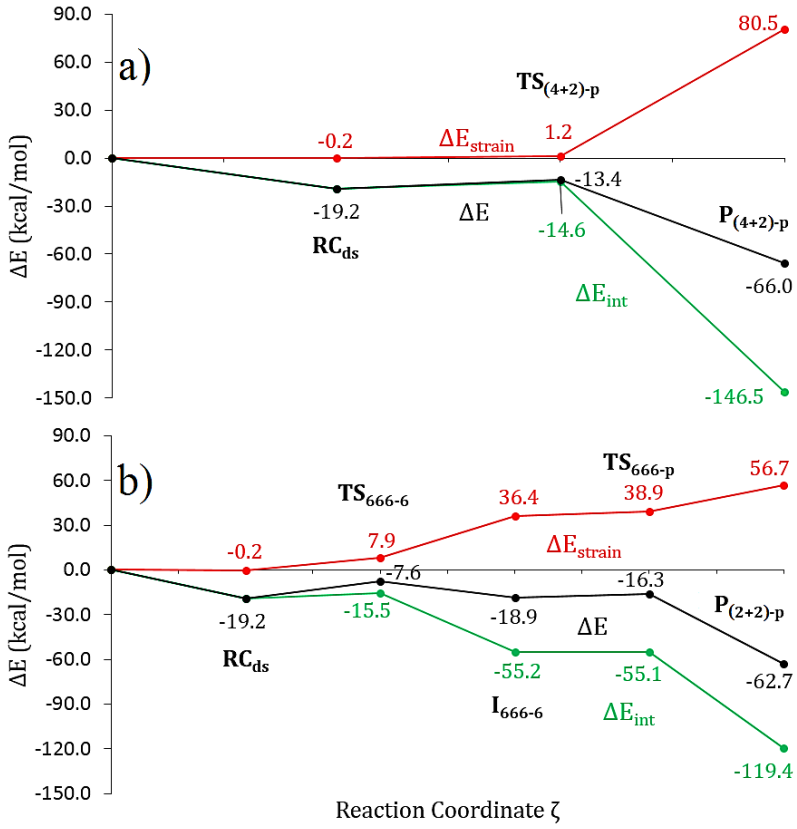

Figure 6. Schematic representation of the activation strain model for the cycloadditions of benzyne to (9,0)-SWCNT. a) Parallel (4+2) BC; b) parallel (2+2) BC. Red, green, and black lines correspond to strain, interaction, and total energies, respectively.

In the ASM, activation energies can be separated into strain and interaction energies, i.e., $\Delta E^{\ddagger} = \Delta E^{\ddagger}_{strain} + \Delta E^{\ddagger}_{int}$. The strain energy $\Delta E^{\ddagger}_{strain}$ is the energy required to deform reactants from their equilibrium geometry into the geometry they acquire in the activated complex; and the transition state interaction $\Delta E^{\ddagger}_{int}$ is the interaction energy between the deformed reactants in the transition state. This model can be extended through all the structures along the reaction coordinate; but here we only focus on the localized stationary points. Figure 6a shows that the (4+2) BC to (9,0)-SWCNT evolves with practically no deformation of the reactants; while for the (2+2) BC involves the formation of intermediate structures in which the reactants are significantly deformed before the ring closure. Despite the fact that (4+2) BC generates a more deformed 6-MR structure (ΔE_{strain} = 80.5 kcal/mol for $\mathbf{P_{(4+2)\text{-}p}}$), we confirm that the formation of the less-strained 4-MR structure produced through the (2+2) BC (ΔE_{strain} = 56.7 kcal/mol for $\mathbf{P_{(2+2)\text{-}p}}$) is not favored due to the

preceding formation of a biradical singly-bonded TS (ΔE_{strain} = 7.9 kcal/mol for **$TS_{666\text{-}6}$**), which cannot compete with the unstrained concerted transition state in the (4+2) BC (ΔE_{strain} = 1.2 kcal/mol for **$TS_{(4+2)\text{-}p}$**). Since the interaction energy is practically the same at the first TS of both BCs (-14.6 and -15.5 kcal/mol for the (4+2) and (2+2) BC, respectively), we conclude that the strain energy determines the course of the reaction. Therefore those cycloadducts produced via a "less strained" reaction pathway will be favored. The same conclusion was reached by Houk and Osuna in a study of a series of (4+2) cycloadditions to PAHs.[95]

It is more illustrative to carefully analyze the TS energy $\Delta E^{\ddagger}$ at the first step of the BC to SWCNTs. Figure 7 shows the evolution of $\Delta E^{\ddagger}_{strain}$ and $\Delta E^{\ddagger}_{int}$ as a function of the diameter and shape of the nanostructures and Table 2 reports some structural parameters for the species under consideration. Observe that benzyne is farther and more tilted for tube-shaped structures with smaller diameters. This result agrees with the Hammond postulate that follows naturally from the ASM and states that more exothermic reactions have TSs with more reactant-like character.[84,96] In order to examine $\Delta E^{\ddagger}$ for C_{60}, the second TSs (i.e. those TSs related to the ring closure, **$TS_{(2+2)}$** and **$TS_{(4+2)}$**) must be taken into consideration since the first TS (**$TS_{566\text{-}6}$**) is common for both BC. Accordingly, it is expected that the reactants in both (4+2) and (2+2) BC are significantly deformed at the TS structures **$TS_{(2+2)}$** and **$TS_{(4+2)}$** because one carbon atom of C_{60} is already covalently linked to one carbon atom of benzyne; thus bringing about relatively larger deformation (when compared to $\Delta E^{\ddagger}_{strain}$ in SWCNTs) which is only compensated by larger values of the interaction energy, as shown in Figure 7. In C_{60}, the (4+2) TS involves a larger deformation by 7.8 kcal/mol as compared to the corresponding (2+2) TS due to the higher C_{60} distortion required for the formation of a 6-MR ring. Furthermore, the interaction energy for the (2+2) TS is more favored by 9.6 kcal/mol; as a result the (4+2) BC to C_{60} is not only disfavored by the structural strain but also by the interaction energy. In the case of the tube-shaped nanostructures, the interaction between reactants at the (2+2) TS is slightly more favored than their counterpart (4+2) by 3.9 to 0.4 kcal/mol. This outcome certainly suggests that the structural strain is the main factor determining the reactivity of the carbon nanostructure. That is to say, for SWCNTs there is more deformation of the reactants in the (2+2) TSs, being from 6.8 to 4.4 kcal/mol more strained than the (4+2) TSs, which in fact hinders the course of the (2+2) BC. The origin of the increased distortion in the TS as the diameter of the SWCNT increases is due to the more pyramidalized carbon atoms in the nanotubes with larger diameters. In Table 2 the distances d_1 and d_2 previously defined in Figure 5b are shown. As the nanotube diameter increases, distances d_1 and d_2 decrease. Consequently, the reacting carbon atoms in the nanotube have to adopt a closer situation to a sp^3-type geometrical configuration, which causes more deformation.

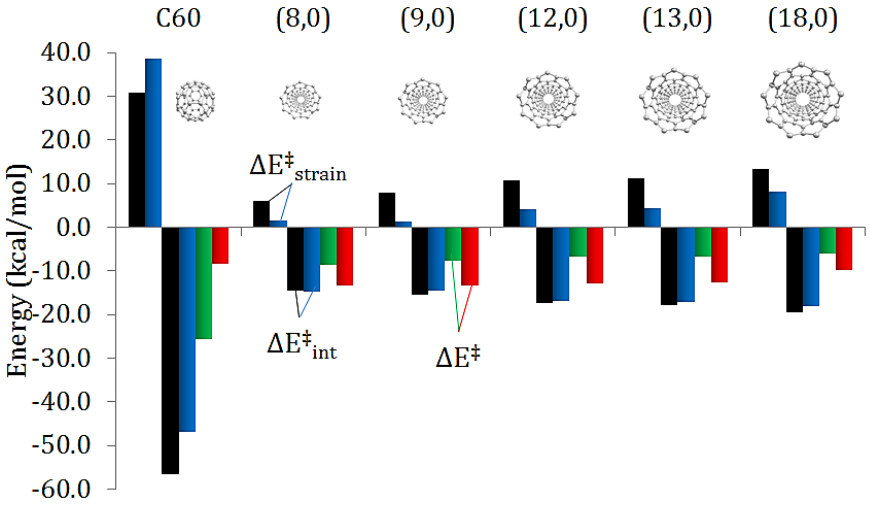

Figure 7. Strain energy $\Delta E^{\ddagger}_{strain}$ (top) and transition state interaction $\Delta E^{\ddagger}_{int}$ (bottom) as a function of the diameter and shape of the carbon nanostructure. Black and blue bars respectively correspond to the (2+2) and (4+2) BC. Green and red bars account for the TS energy ($\Delta E^{\ddagger} = \Delta E^{\ddagger}_{strain} + \Delta E^{\ddagger}_{int}$) for the (2+2) and (4+2) BC, respectively. In the case of C_{60}, the values correspond to **TS**$_{(2+2)-5,6}$ and **TS**$_{(4+2)-5}$. For SWCNTs, the first (2+2) TS is compared to the (4+2) TS.

The nearly null variation in $\Delta E^{\ddagger}_{int}$ as a function of the diameter of the nanotube observed in Figure 7 can be partially explained in terms of Frontier Molecular Orbital (FMO) theory. In Table S4 in the Supporting Information it is reported HOMO and LUMO energies of each one of the fragments (i.e. benzyne and (*n*,0)-SWCNT) interacting in the corresponding TS for both (4+2) and (2+2) BCs. We observe no significant variation of the HOMO and LUMO energies of the interacting fragments when comparing the smallest- against the largest-diameter nanotube under study; a result that is attributed to the negligible variation in $\Delta E^{\ddagger}_{int}$ as the curvature of the structure is increased, thus resembling our conclusions that the structural deformation is indeed the main factor determining the chemoselectivity of the cycloadditions with benzyne.

Table 2. Some structural parameters of the main transition state structures for the cycloaddition of benzyne to different carbon nanostructures. Distances in Å and angles in degrees.

	(2+2)		**(4+2)**		
	d	φ	d_1	d_2	θ
C_{60}[a]	1.505	123.1	1.575	2.302	-
(8,0)	2.065	74.7	2.498	2.698	134.2
(9,0)	2.005	66.2	2.498	2.854	139.1
(12,0)	1.949	62.1	2.258	2.811	149.5
(13,0)	1.936	61.8	2.258	2.791	149.8
(18,0)	1.925	60.9	2.165	2.750	150.4

[a] Structures are **TS**$_{(2+2)-5,6}$ and **TS**$_{(4+2)-5}$

Conclusions

In this work, we have studied the mechanisms for the sidewall cycloadditions of benzyne to different nanostructures of carbon to account for the chemoselectivity ((2+2) vs (4+2) additions) and regioselectivity ([5,6] vs [6,6] in fullerenes or parallel vs. oblique addition in nanotubes) of the reaction. The (2+2) additions are preferred over the (4+2) for C_{60} and for the armchair SWCNTs of small diameter, whereas the zig-zag SWCNTs and the armchair SWCNTs of large diameter favor the (4+2) attack.[54] From the results obtained in the present work and previous studies (the following conclusions 2 and 4 are extracted from refs. [74] and 55, respectively) we reach the following picture for the benzyne cycloaddition to carbon nanostructures of different curvature:

1. In C_{60}, once the biradical singly-bonded intermediate structure is formed, the rotation of benzyne in such an intermediate leads to the formation of closed-cage (2+2) cycloadducts in a practically barrierless process. The attack on a [6,6] bond of the cage produces the most kinetically and thermodynamically preferred reaction pathway, in good agreement with experimental evidence. Nonetheless, the attack on a [5,6] bond kinetically competes with the attack on a [6,6] bond; therefore the corresponding [5,6] product can be also observed as suggested in previous reports based on indirect experimental evidences.
2. For the $X_3N@C_{80}$ (X = Sc, Y) endohedral metallofullerenes[74] the situation is similar. The (2+2) addition is preferred over the (4+2) one and the [5,6] and [6,6] attacks compete, although the former is favored in the case of $Sc_3N@C_{80}$.
3. For zig-zag SWCNTs, the sidewall (4+2) cycloaddition of benzyne in the parallel position to the SWCNTs is the most kinetically and thermodynamically preferred reaction pathway. When the diameter of the zig-zag SWCNTs increases, the energy barrier increases and the exothermicity of the reaction decreases.
4. In armchair SWCNTs,[55] the (4+2) cycloaddition of benzyne in an oblique position is the most favorable for large diameters of the nanotube. For small diameters, the oblique (2+2) addition is preferred thermodynamically, whereas kinetically the most favorable attack is the one in the perpendicular (or orthogonal) position. Like zig-zag nanotubes, when the diameter of the armchair SWCNTs increases, the reaction becomes less exothermic and the energy barrier increases.

The changes in chemoselectivity and regioselectivity can be explained in terms of structural strain and interaction between reactants. Thus, the sidewall (4+2) cycloaddition to zig-zag SWCNTs evolves with practically no structural deformation making it the most favorable reaction pathway.

Acknowledgements

The following organizations are thanked for financial support: the Spanish government (MINECO, projects number CTQ2014-54306-P, CTQ2014-59212-P, and CTQ2013-48252-P), the Generalitat de Catalunya (project number 2014SGR931, Xarxa de Referència en Química Teòrica i Computacional, and ICREA Academia 2014 prize to M. S.), and the FEDER fund (European Fund for Regional Development) for the grant UNGI10-4E-801. We thank the National Research School Combination - Catalysis (NRSC-C), and The Netherlands Organization for Scientific Research (NWO/CW and NWO/NCF). J.P.M. gratefully acknowledges a Ph.D. fellowship (register/application no. 217067/312543) from the Mexican National Council of Science and Technology (CONACYT). S.O. thanks the MINECO for the Juan de la Cierva fellowship and the European Community for the CIG project (FP7-PEOPLE-2013-CIG-630978). The authors are also grateful to the computer resources, technical expertise, and assistance provided by the Barcelona Supercomputing Center - Centro Nacional de Supercomputación. Excellent service by the Stichting Academisch Rekencentrum Amsterdam (SARA) and the Centre de Serveis Científics i Acadèmics de Catalunya (CESCA) is gratefully acknowledged.

Supporting Information

The construction of conventional single-walled carbon nanostructures (i.e. non-Clar structures) is depicted in Figure S1. A detailed explanation of how they are built is also provided. In Figure S2, the four possible additions to conventional structure of (9,0)-SWCNT are depicted. Table S1 contains a comparison between reaction energies (considering reactants, reactant complex, transition states, and cycloadducts for both (4+2) and (2+2) additions) obtained with this model of (9,0)-SWCNT and the one constructed under the Clar theory. Detailed discussion is also given. In Table S2 the performance of the size of the model implemented to construct (9,0)-SWCNT is assessed by comparing reaction energies calculated for models constructed with 3 and 6 unit cells for both conventional and Clar nanotube structures. In Figures S3 and S4, we report the potential energy surface for noncovalent interactions between benzyne and C_{60}. In Figure S5, the potential energy surface corresponding to the rupture of the attacked [5,6] bond of C_{60} in the (2+2) cycloadduct is shown. Linear transits around the transition state structures involving the ring closure of the (2+2) and (4+2) cycloadditions of benzyne to (9,0)-SWCNT are reported in Figures S6 and S7, respectively. The cycloadditions of benzyne to benzenoid and non-benzenoid reaction sites are described in Figure S8. Table S3 compares the reaction energies calculated on a benzenoid reaction site with the analogous non-benzenoid ones. In Table S4, HOMO and LUMO absolute energies are given for interacting fragments in the first TS structure of the benzyne cycloadditions. Two examples are reported, orbital energies for fragments benzyne and (8,0)-SWCNT, and benzyne and (18,0)-SWCNT. Bibliography related to the construction of single-walled carbon nanotubes is also reported. At the end of the document, Cartesian coordinates and Gibbs and electronic energies are provided for all the optimized structures of reactants, reactant complexes, transition states (with their respective imaginary frequency), and cycloadducts; including structures derived from conventional nanotube models and non-benzenoid centers, as well as 6-unit-cells structures.

References

(1) Yang, Z.; Ren, J.; Zhang, Z.; Chen, X.; Guan, G.; Qiu, L.; Zhang, Y.; Peng, H. *Chem. Rev.* **2015**, *115*, 5159–5223.

(2) Su, D. S.; Perathoner, S.; Centi, G. *Chem. Rev.* **2013**, *113*, 5782–5816.

(3) Delgado, J. L.; Herranz, M.; Martín, N. *J. Mater. Chem.* **2008**, *18*, 1417–1426.

(4) Li, Z.; Liu, Z.; Sun, H.; Gao, C. *Chem. Rev.* **2015**, *115*, 7046–7117.

(5) Kroto, H. W.; Heath, J. R.; O'Brien, S. C.; Curl, R. F.; Smalley, R. E. *Nature* **1985**, *318*, 162–163.

(6) Kroto, H. W.; Allaf, A. W.; Balm, S. P. *Chem. Rev.* **1991**, *91*, 1213–1235.

(7) Thilgen, C.; Diederich, F. *Chem. Rev.* **2006**, *106*, 5049–5135.

(8) Jennepalli, S.; Pyne, S. G.; Keller, P. A. *RSC Adv.* **2014**, *4*, 46383–46398.

(9) Tong, J.; Zimmerman, M. C.; Li, S.; Yi, X.; Luxenhofer, R.; Jordan, R.; Kabanov, A. V. *Biomaterials* **2011**, *32*, 3654–3665.

(10) Li, C.-Z.; Yip, H.-L.; Jen, A. K.-Y. *J. Mater. Chem.* **2012**, *22*, 4161–4177.

(11) Babu, S. S.; Praveen, V. K.; Ajayaghosh, A. *Chem. Rev.* **2014**, *114*, 1973–2129.

(12) Martín, N.; Sánchez, L.; Illescas, B.; Pérez, I. *Chem. Rev.* **1998**, *98*, 2527–2548.

(13) Yang, Y. H.; Li, W. Z. *Appl. Phys. Lett.* **2011**, *98*, 041901.

(14) Treacy, M. M. J.; Ebbesen, T. W.; Gibson, J. M. *Nature* **1996**, *381*, 678–680.

(15) Thostenson, E.; Li, C.; Chou, T. *Compos. Sci. Technol.* **2005**, *65*, 491–516.

(16) Pop, E.; Mann, D.; Wang, Q.; Goodson, K.; Dai, H. *Nano Lett.* **2006**, *6*, 96–100.

(17) Ouyang, M.; Huang, J.-L.; Lieber, C. M. *Acc. Chem. Res.* **2002**, *35*, 1018–1025.

(18) Itkis, M. E.; Niyogi, S.; Meng, M. E.; Hamon, M. A.; Hu, H.; Haddon, R. C. *Nano Lett.*

2002, *2*, 155–159.

(19) Kataura, H.; Kumazawa, Y.; Maniwa, Y.; Umezu, I.; Suzuki, S.; Ohtsuka, Y.; Achiba, Y. *Synth. Met.* **1999**, *103*, 2555–2558.

(20) Yan, Y.; Miao, J.; Yang, Z.; Xiao, F.-X.; Yang, H. Bin; Liu, B.; Yang, Y. *Chem. Soc. Rev.* **2015**, *44*, 3295–3346.

(21) Saito, N.; Haniu, H.; Usui, Y.; Aoki, K.; Hara, K.; Takanashi, S.; Shimizu, M.; Narita, N.; Okamoto, M.; Kobayashi, S.; Nomura, H.; Kato, H.; Nishimura, N.; Taruta, S.; Endo, M. *Chem. Rev.* **2014**, *114*, 6040–6079.

(22) Dyke, C. A.; Tour, J. M. *J. Phys. Chem. A* **2004**, *108*, 11151–11159.

(23) Sun, Y.-P.; Fu, K.; Lin, Y.; Huang, W. *Acc. Chem. Res.* **2002**, *35*, 1096–1104.

(24) Prato, M.; Kostarelos, K.; Bianco, A. *Acc. Chem. Res.* **2008**, *41*, 60–68.

(25) Marcus, Y.; Smith, A. L.; Korobov, M. V.; Mirakyan, A. L.; Avramenko, N. V.; Stukalin, E. B. *J. Phys. Chem. B* **2001**, *105*, 2499–2506.

(26) Duque, J. G.; Parra-Vasquez, A. N. G.; Behabtu, N.; Green, M. J.; Higginbotham, A. L.; Price, B. K.; Leonard, A. D.; Schmidt, H. K.; Lounis, B.; Tour, J. M.; Doorn, S. K.; Cognet, L.; Pasquali, M. *ACS Nano* **2010**, *4*, 3063–3072.

(27) Criado, A.; Gómez-Escalonilla, M. J.; Fierro, J. L. G.; Urbina, A.; Peña, D.; Guitián, E.; Langa, F. *Chem. Commun.* **2010**, *46*, 7028–7030.

(28) McHedlov-Petrossyan, N. O. *Chem. Rev.* **2013**, *113*, 5149–5193.

(29) Tasis, D.; Tagmatarchis, N.; Bianco, A.; Prato, M. *Chem. Rev.* **2006**, *106*, 1105–1136.

(30) Yang, T.; Zhao, X.; Nagase, S. *J. Comput. Chem.* **2013**, *34*, 2223–2232.

(31) Martín, N. *Chem. Commun.* **2006**, 2093–2104.

(32) Chaur, M. N.; Melin, F.; Ortiz, A. L.; Echegoyen, L. *Angew. Chem. Int. ed.* **2009**, *48*, 7514–7538.

(33) Yamada, M.; Akasaka, T.; Nagase, S. *Acc. Chem. Res.* **2010**, *43*, 92–102.

(34) Osuna, S.; Swart, M.; Solà, M. *Phys. Chem. Chem. Phys.* **2011**, *13*, 3585–35603.

(35) Popov, A. A.; Yang, S.; Dunsch, L. *Chem. Rev.* **2013**, *113*, 5989–6113.

(36) Kumar, I.; Rana, S.; Cho, J. W. *Chem. - Eur. J.* **2011**, *17*, 11092–11101.

(37) Hoke, S. H.; Molstad, J.; Dilettato, D.; Jay, M. J.; Carlson, D.; Kahr, B.; Cooks, R. G. *J. Org. Chem.* **1992**, *57*, 5069–5071.

(38) Ishida, T.; Shinozuka, K.; Nogami, T.; Sasaki, S.; Iyoda, M. *Chem. Lett.* **1995**, *24*, 317–318.

(39) Nakamura, Y.; Takano, N.; Nishimura, T.; Yashima, E.; Sato, M.; Kudo, T.; Nishimura, J. *Org. Lett.* **2001**, *3*, 1193–1196.

(40) Kim, G.; Lee, K. C.; Kim, J.; Lee, J.; Lee, S. M.; Lee, J. C.; Seo, J. H.; Choi, W.-Y.; Yang, C. *Tetrahedron* **2013**, *69*, 7354–7359.

(41) Darwish, A. D.; Abdul-Sada, A. K.; Langley, G. J.; Kroto, H. W.; Taylor, R.; Walton, D. R. M. *J. Chem. Soc. Chem. Commun.* **1994**, 2133–2134.

(42) Darwish, A. D.; Avent, A. G.; Taylor, R.; Walton, D. R. M. *J. Chem. Soc. Perkin Trans. 2* **1996**, 2079–2084.

(43) Meier, M. S.; Wang, G.-W.; Haddon, R. C.; Brock, C. P.; Lloyd, M. A.; Selegue, J. P. *J. Am. Chem. Soc.* **1998**, *120*, 2337–2342.

(44) Lu, X.; Xu, J.; He, X.; Shi, Z.; Gu, Z. *Chem. Mater.* **2004**, *16*, 953–955.

(45) Lu, X.; Nikawa, H.; Tsuchiya, T.; Akasaka, T.; Toki, M.; Sawa, H.; Mizorogi, N.; Nagase, S. *Angew. Chemie* **2010**, *122*, 604–607.

(46) Li, F.-F.; Pinzón, J. R.; Mercado, B. Q.; Olmstead, M. M.; Balch, A. L.; Echegoyen, L. *J. Am. Chem. Soc.* **2011**, *133*, 1563–1571.

(47) Rivera-Nazario, D. M.; Pinzón, J. R.; Stevenson, S.; Echegoyen, L. A. *J. Phys. Org. Chem.* **2013**, *26*, 194–205.

(48) Wang, G.-W.; Liu, T.-X.; Jiao, M.; Wang, N.; Zhu, S.-E.; Chen, C.; Yang, S.; Bowles, F. L.; Beavers, C. M.; Olmstead, M. M.; Mercado, B. Q.; Balch, A. L. *Angew. Chem., Int. ed.* **2011**, *50*, 4658–4662.

(49) Fagan, S. B.; da Silva, A. J. R.; Mota, R.; Baierle, R. J.; Fazzio, A. *Phys. Rev. B* **2003**, *67*, 033405.

(50) Bettinger, H. F.; Kudin, K. N.; Scuseria, G. E. *J. Am. Chem. Soc.* **2001**, *123*, 12849–

12856.

(51) Osuna, S.; Torrent-Sucarrat, M.; Solà, M.; Geerlings, P.; Ewels, C. P.; Lier, G. Van. *J. Phys. Chem. C* **2010**, *114*, 3340–3345.

(52) Ogunro, O. O.; Nicolas, C. I.; Mintz, E. A.; Wang, X.-Q. *ACS Macro Lett.* **2012**, *1*, 524–528.

(53) Globus, A.; Bauschlicher, C. W.; Han, J.; Jaffe, R. L.; Levit, C.; Srivastava, D. *Nanotechnology* **1998**, *9*, 192–199.

(54) Criado, A.; Vizuete, M.; Gómez-Escalonilla, M. J.; García-Rodriguez, S.; Fierro, J. L. G.; Cobas, A.; Peña, D.; Guitián, E.; Langa, F. *Carbon N. Y.* **2013**, *63*, 140–148.

(55) Yang, T.; Zhao, X.; Nagase, S. *Org. Lett.* **2013**, *15*, 5960–5963.

(56) te Velde, G.; Bickelhaupt, F. M.; Baerends, E. J.; Fonseca Guerra, C.; van Gisbergen, S. J. A.; Snijders, J. G.; Ziegler, T. *J. Comput. Chem.* **2001**, *22*, 931–967.

(57) Snijders, J. G.; Swart, M. *Theor. Chem. Acc.* **2003**, *110*, 34–41.

(58) Swart, M.; Snijders, J. G. *Theor. Chem. Acc.* **2004**, *111*, 56–56.

(59) Lenthe, E. van; Baerends, E. J.; Snijders, J. G. *J. Chem. Phys.* **1993**, *99*, 4597.

(60) van Lenthe, E.; van Leeuwen, R.; Baerends, E. J.; Snijders, J. G. *Int. J. Quantum Chem.* **1996**, *57*, 281–293.

(61) Becke, A. D. *Phys. Rev. A* **1988**, *38*, 3098–3100.

(62) Perdew, J. *Phys. Rev. B* **1986**, *33*, 8822–8824.

(63) Grimme, S. *J. Comput. Chem.* **2006**, *27*, 1787–1799.

(64) Osuna, S.; Swart, M.; Solà, M. *J. Phys. Chem. A* **2011**, *115*, 3491–3496.

(65) Swart, M.; Bickelhaupt, F. M. *J. Comput. Chem.* **2008**, *29*, 724–734.

(66) Swart, M.; Bickelhaupt, F. M. *Int. J. Quantum Chem.* **2006**, *106*, 2536–2544.

(67) Cao, Y.; Osuna, S.; Liang, Y.; Haddon, R. C.; Houk, K. N. *J. Am. Chem. Soc.* **2013**, *135*, 17643–17649.

(68) Kawase, T.; Kurata, H. *Chem. Rev.* **2006**, *106*, 5250–5273.

(69) Pincak, R.; Pudlak, M. **2007**, arXiv:cond – mat/0703580v1 [cond – mat.mtrl – sci].

(70) Ando, T. *J. Phys. Soc. Japan* **2000**, *69*, 1757–1763.

(71) Smotlacha, J.; Pincak, R.; Pudlak, M. *Eur. Phys. J. B* **2011**, *84*, 255–264.

(72) Pincak, R.; Smotlacha, J.; Pudlak, M. *Eur. Phys. J. B* **2015**, *88*, 17.

(73) Pincak, R.; Smotlacha, J.; Osipov, V. A. *Phys. B Condens. Matter* **2015**, *475*, 61–65.

(74) Yang, T.; Nagase, S.; Akasaka, T.; Poblet, J. M.; Houk, K. N.; Ehara, M.; Zhao, X. *J. Am. Chem. Soc.* **2015**, *137*, 6820–6828.

(75) Cases, M.; Duran, M.; Mestres, J.; Martín, N.; Solà, M. *Fullerenes for the New Millennium*, Vol. 11.; Kamat, P. V., Kadish, K. M., Guldi, D. M., Eds.; The Electrochemical Society Inc., Pennington, 2011.

(76) Matsuo, Y.; Tahara, K.; Nakamura, E. *Org. Lett.* **2003**, *5*, 3181–3184.

(77) Baldoni, M.; Sgamellotti, A.; Mercuri, F. *Org. Lett.* **2007**, *9*, 4267–4270.

(78) Baldoni, M.; Selli, D.; Sgamellotti, A.; Mercuri, F. *J. Phys. Chem. C* **2009**, *113*, 862–866.

(79) Clar, E. *The Aromatic Sextet*; Wiley: New York, 1972.

(80) Solà, M. *Front. Chem.* **2013**, *1*, 22.

(81) Martín-Martínez, F. J.; Melchor, S.; Dobado, J. A. *Phys. Chem. Chem. Phys.* **2011**, *13*, 12844–12857.

(82) Garcia-Borràs, M.; Osuna, S.; Luis, J. M.; Swart, M.; Solà, M. *Chem. Soc. Rev.* **2014**, *43*, 5089–5105.

(83) Martín-Martínez, F. J.; Melchor, S.; Dobado, J. A. *Org. Lett.* **2008**, *10*, 1991–1994.

(84) Zhao, J.; Balbuena, P. B. *J. Phys. Chem. C* **2008**, *112*, 3482–3488.

(85) Pierrefixe, S. C. A. H.; Bickelhaupt, F. M. *Chem. - Eur. J.* **2007**, *13*, 6321–6328.

(86) Pierrefixe, S. C. A. H.; Bickelhaupt, F. M. *Chem. - Eur. J.* **2007**, *13*, 8371–8371.

(87) Hammouri, M.; Jha, S. K.; Vasiliev, I. *J. Phys. Chem. C* **2015**, *119*, 18719–18728.

(88) van Zeist, W.-J.; Bickelhaupt, F. M. *Org. Biomol. Chem.* **2010**, *8*, 3118–3127.

(89) Bickelhaupt, F. M. *J. Comput. Chem.* **1999**, *20*, 114–128.

(90) Fernández, I.; Bickelhaupt, F. M. *Chem. Soc. Rev.* **2014**, *43*, 4953–4967.

(91) Wolters, L. P.; Bickelhaupt, F. M. *WIREs Comput. Mol. Sci.* **2015**, *5*, 324–343.

(92) Houk, K. N.; Gandour, R. W.; Strozier, R. W.; Rondan, N. G.; Paquette, L. A. *J. Am. Chem. Soc.* **1979**, *101*, 6797–6802.

(93) Ess, D. H.; Houk, K. N. *J. Am. Chem. Soc.* **2007**, *129*, 10646–10647.

(94) Cao, Y.; Liang, Y.; Zhang, L.; Osuna, S.; Hoyt, A.-L. M.; Briseno, A. L.; Houk, K. N. *J. Am. Chem. Soc.* **2014**, *136*, 10743–10751.

(95) Osuna, S.; Houk, K. N. *Chem. - Eur. J.* **2009**, *15*, 13219–13231.

(96) Hammond, G. S. *J. Am. Chem. Soc.* **1955**, *77*, 334–338.

TABLE OF CONTENTS